Cancer Immunotherapy by Interleukin-21: Potential Treatment Strategies Evaluated in a Mathematical Model

Antonio Cappuccio, Moran Elishmereni, and Zvia Agur

Institute for Medical Biomathematics, Bene-Ataroth, Israel

Abstract

The newly characterized interleukin (IL)-21 plays a central role in the transition from innate immunity to adaptive immunity and shows substantial tumor regression in mice. IL-21 is now developed as a cancer immunotherapeutic drug, but conditions for efficacious therapy, and the conflicting immunostimulatory and immunoinhibitory influence of the cytokine, are yet to be defined. We studied the effects of IL-21 on tumor eradication in a mathematical model focusing on natural killer (NK) cell–mediated and $CD8^+$ T-cell-mediated lysis of tumor cells. Model parameters were estimated using results in tumor-bearing mice treated with IL-21 via cytokine gene therapy (CGT), hydrodynamics-based gene delivery (HGD), or standard interval dosing (SID). Our model accurately retrieved experimental growth dynamics in the nonimmunogenic B16 melanoma and the immunogenic MethA and MCA205 fibrosarcomas, showing a strong dependence of the NK-cell/$CD8^+$ T-cell balance on tumor immunogenicity. Moreover, in melanoma, simulations of CGT-like dosing regimens, dynamically determined according to tumor mass changes, resulted in efficient disease elimination. In contrast, in fibrosarcoma, such a strategy was not superior to that of fixed dosing regimens, HGD or SID. Our model supports clinical use of IL-21 as a potent stimulator of cellular immunity against cancer, and suggests selecting the immunotherapy strategy according to tumor immunogenicity. Nonimmunogenic tumors, but not highly immunogenic tumors, should be controlled by IL-21 dosing, which depends on tumor mass at the time of administration. This method imitates, yet amplifies, the natural anticancer immune response rather than accelerates only one of the response arms in an unbalanced manner. (Cancer Res 2006; 66(14): 7293-300)

Introduction

Despite the existence of numerous pathways in anticancer immunity, malignant cells effortlessly escape immune surveillance. The late and insufficient immune responses to tumor challenge and the wide array of immune evasion strategies employed by cancerous cells enable an undisturbed disease progression (1). It seems, then, that artificial modulation of the natural immune response is necessary for an adequate immune attack against tumor cells. Specifically, rapid instigation of tumor-specific immunity and enhanced killing potential of immune effectors are essential for successful eradication of cancer (1).

The interleukin (IL)-2 family of cytokines is well known for its central involvement in the regulation of acquired immunity. A recently identified member of this family, sharing homology with IL-2, IL-4, and IL-15, is IL-21, a product of activated $CD4^+$ T-helper cells (2). In both *in vitro* and *in vivo* studies, IL-21 directly modulates number and function of natural killer (NK) cells, dendritic cells, and lymphocytes (3, 4). Importantly, IL-21 enhances effector cell-mediated lysis of tumor cells, induces efficient antitumor immune memory, and significantly minimizes angiogenic and metastatic processes in numerous tumors (2, 5–10). The potent antitumor effect of IL-21 is attributed to its role in facilitating the transition from innate NK-cell responses to acquired cytotoxic $CD8^+$ T-cell responses. This is presumably achieved by inhibiting the former and stimulating the latter and by enhancing the cytotoxic activity of both cell-types (2, 3, 11, 12).

The immunostimulatory effects of IL-21 motivated its development as an immunotherapeutic agent for the treatment of cancer. The minimal toxicity of IL-21 to mice compared with IL-2, IL-15, and other immunotherapeutic factors (2, 5, 13, 14) further supports its clinical applicability. Yet, theoretically, the stimulatory effect of IL-21 on $CD8^+$ T cells can be counterbalanced by its inhibitory influence on NK cells and other factors of cell-mediated immunity (2, 11). These contradicting effects may limit the IL-21-induced antitumor response. Therefore, it seems mandatory to analyze the IL-21 net immunotherapeutic power in different oncological scenarios before the establishment of an immunotherapeutic policy for this molecule.

Such analysis is enabled by biomathematically modeling IL-21 interactions with the involved immunologic and pathologic processes. Biomathematical models have been employed previously for analyzing the effect of environmental disturbances on population survival, in general, and the effect of the interdosing intervals of the drug on chemotherapy efficacy/toxicity ratio, in particular (15). Analysis of individual tumor growth patterns in xenografted human ovary carcinoma spheroids was also possible by biomathematical modeling of complex angiogenesis-related processes (16). Another mathematical model describing detailed thrombopoiesis was employed for optimizing treatment strategies of thrombopoietin. The accuracy of the qualitative and quantitative predictions of the model was prospectively validated in the preclinical setting (17). Recent mathematical models of tumor-immune interactions emphasize the role of certain effectors in anticancer responses and evaluate efficacy of immunotherapy in the context of tumor challenge (18, 19).

In the current study, the antitumor effects of IL-21 under different oncological settings are evaluated in a mathematical model of the underlying biological processes. Following the calibration of the model using published experimental data, we investigate IL-21 treatment strategies and suggest efficacious regimens for eradicating or substantially attenuating tumor mass. A beneficial treatment should maximize IL-21-stimulated activation of adaptive immunity and, concurrently, minimize its

Note: Supplementary data for this article are available at Cancer Research Online (http://cancerres.aacrjournals.org/).

Requests for reprints: Zvia Agur, Institute for Medical Biomathematics, P.O. Box 282, 10 HaTe'ena Street, Bene-Ataroth 60991, Israel. Phone: 972-3-9733075; Fax: 972-3-9733410; E-mail: agur@imbm.org.

doi:10.1158/0008-5472.CAN-06-0241

negative effects on innate immunity. These conflicting aims for different tumor dynamics and immunogenicity levels will be investigated in this work.

Materials and Methods

Our mathematical model for IL-21 immunotherapy is based on the state-of-the-art biology of the system, and its parameters were evaluated by experimental results through the Matlab curve-fitting toolbox and numerical analysis. Fourth-order Runge-Kutta integration of the equations was implemented by Matlab programming (see Supplementary Data) to enable model simulations for retrieving experimental behavior and evaluating putative therapeutic scenarios.

Biological Assumptions and Mathematical Model

As IL-21 has a central role in mediating the transition from initial NK-cell immunity to secondary T-cell immunity, this bipolar mechanism is highlighted in our model, where the effects of IL-21 on NK and $CD8^+$ T cells are taken to be direct and independent of other factors (4–10, 13, 14, 20–25). Importantly, the model focuses on the IL-21 contribution to cellular immunity and implicitly refers to the naturally induced responses (in the non-IL-21 setting) by subsuming them into the baseline (control) tumor growth. Thus, factors normally influencing NK and $CD8^+$ T cells (such as dendritic cells, secondary chemokines, and reciprocal interactions between the effectors) are not explicitly incorporated in this stage. Due to their minor contribution in the IL-21-associated anticancer response and their transient and low secretion of IL-21 compared with therapeutic doses (2, 5, 6, 13), $CD4^+$ T helpers are neglected as well.

The IL-21-mediated immunity is evaluated here on a short time-scale of weeks and is restricted to primary tumor challenge. Additionally, possible inflammation-related consequences of IL-21 therapy are neglected in this initial model, as corroborated by the minor toxic effects reported in the murine setting (2, 5–7).

Two classes of administration methods are examined here: drug application associated with tumor mass (Fig. 1*A*) and drug application being independent of tumor mass (Fig. 1*B*). The first method is represented by cytokine gene therapy (CGT), in which genetically modified tumor cells continuously secrete IL-21 (5, 6). The second administration method is represented by hydrodynamics-based gene delivery (HGD) of DNA plasmids encoding large amounts of murine IL-21 or by standard interval dosing (SID) of recombinant murine IL-21 (7, 13).

A concise mathematical description of the above assumptions includes a system of six ordinary differential equations (ODE) describing IL-21 concentration in the organism at any moment (Eq. A), population dynamics of NK cells in the spleen (Eq. B), population dynamics of specific antitumor $CD8^+$ T cells in the lymph nodes (Eq. C), an element facilitating $CD8^+$ T-cell memory (Eq. D), a cytotoxic protein affecting tumor lysis (Eq. E), and tumor mass at any moment (Eq. F):

$$\dot{u} = input - \mu_1 u \tag{A}$$

$$\dot{x} = r_1 x\left(1 - \frac{x}{h_1(u)}\right) \tag{B}$$

$$\dot{y} = r_2 y\left(1 - \frac{y}{h_2(m)}\right) \tag{C}$$

$$\dot{m} = au - \mu_2 m \tag{D}$$

$$\dot{p} = \frac{b_1 u}{b_2 + u} - \mu_3 p \tag{E}$$

$$\dot{n} = g(n) - k_1 pxn - k_2 pyn \tag{F}$$

where

$$h_1(u) = \frac{p_1 u + p_2}{u + q_1} \tag{G}$$

and

$$h_2(m) = h_2(0) + \frac{\sigma m}{1 + \frac{m}{D}}. \tag{H}$$

IL-21 dynamics. In our model, the concentration of IL-21, u, is measured in units of ng/mL by Eq. A, the initial condition being $u_0 = u(t = 0)$. The clearance rate is μ_1, and the exogenous IL-21 application route is the function *input* (Fig. 1): In the first case (CGT), *input* is taken as proportional to the total number of genetically engineered tumor cells, n. This forms Eq. A as

$$\dot{u} = hn - \mu_1 u. \tag{I}$$

In contrast, the latter cases (HGD or SID) use a pulse-like function centered at the application time (see Parameter Estimation).

NK-cell dynamics. The splenic NK population, x, is assumed to grow according to the logistic growth law (Eq. B), where r_1 is the growth rate, and the IL-21 effect on NK-cell population size is incorporated in $h_1(u)$, the carrying capacity in the logistic function. The latter component (Eq. G) is a linear rational function that satisfies basic biological requirements: Firstly, the mean number of splenic NK cells in normal conditions is constant, given by $x_0 = h_1$ ($u = 0$). This accounts for the high availability of NK cells in stable health conditions (1, 26). Secondly, the IL-21 effect on the growth of mouse NK cells is apparently biphasic: at low doses NK proliferation is stimulated, whereas at higher doses it is inhibited (11, 27). However, as the positive effect on NK expansion is short-lived and observed mainly in the absence or low concentrations of other ILs (11) and hence irrelevant to *in vivo* conditions, we address only the negative effect of IL-21. Thus, the model considers IL-21-imposed reduction of NK cells in a dose-dependent manner, and $h_1(u)$ is selected as a monotonic decreasing function of IL-21. Thirdly, a saturation in the NK population is included, so it cannot decrease below the normal threshold $x_{\min}$, the steady state for NK dynamics for $u = \infty$. This limit is set within the normative biological range.

The above characteristics serve as constraints for the parameters p_1, p_2, and q_1. In particular, the relations $x_0 = p_2 / q_1$ and $p_1 = x_{\min}$ can be derived. In allowing p_2 and q_1 to vary while maintaining their ratio constantly equal to x_0, a one-parameter family of curves can be generated. A subsequent fit enables to estimate the value of this parameter that interpolates the experimental behavior (see Parameter Estimation).

$CD8^+$ T-cell dynamics. The IL-21-mediated expansion of naive and activated $CD8^+$ T cells in both nonstimulated (4, 28–30) and stimulated (5, 7, 13) conditions suggests a robust influence of the cytokine on the carrying capacity of these cells. $CD8^+$ T cells persist for many weeks after IL-21 application, allowing long-term protection against subsequent tumor inoculation (5, 7, 20, 22, 30). Distinct memory phenotypes observed in T-cell subsets following exposure to IL-21 (31) support this durable effect. Hence, we introduce an indirect factor m as an IL-21 dose-dependent product, which acts on $CD8^+$ T-cell expansion to enable a prolonged adaptive response of these cells even after complete IL-21 clearance. Consequently, the dynamics of m are given by Eq. D, where a is the proportionality constant and μ_2 is the clearance rate, the reciprocal of which is a measure of the duration of the $CD8^+$ T-cell response.

The tumor-specific $CD8^+$ T subset in the lymph nodes, denoted by y, is therefore described by Eq. C, with the initial condition, $y_0 = h_2$ ($m = 0$), representing the number of such cells in an untreated setting. The logistic growth rate is r_2, and the carrying capacity, h_2, is a function of the memory factor m, given by Eq. H. The coefficient σ relates the growth of the carrying capacity to the memory factor (Eq. D). The actual limitation for specific $CD8^+$ T cells, substantiated by recognized inhibitory functions of T-regulatory cells and Th2 cytokines (32), is enclosed in D. To maintain

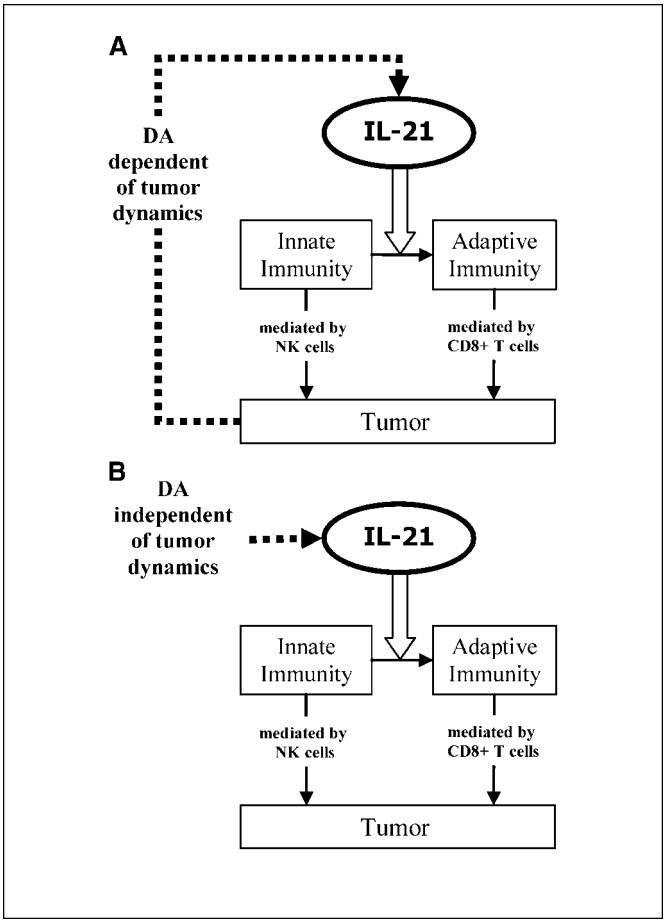

Figure 1. Flow diagram of the modeled IL-21-induced antitumor mechanism. IL-21 accelerates the transition from innate NK-cell-mediated immunity to adaptive $CD8^+$ T-cell-mediated immunity, thereby eliciting an efficient immune response against target cells. Administration of IL-21 is considered in two scenarios: dependent of tumor dynamics (*A*) or independent of tumor dynamics (*B*). The recommended strategy of choice takes tumor immunogenicity into account.

the system within realistic biological ranges, we assume that this expansion has an upper bound $y_\infty = h_2(0) + \sigma D$.

Cytotoxic protein dynamics. Our model also accounts for the IL-21-mediated increase in effector-cell killing potential by assuming existence of cytotoxic proteins, such as perforin and IFN-γ (2, 3, 10, 12, 33). This effect is assumed to be IL-21 dose-dependent (5, 7, 13, 21, 28), coinciding with the biological function of IL-21 as a ligand for the signaling cascade resulting in cytotoxic protein secretion. Because both $CD8^+$ T and NK cells exert their effects via the same cytotoxic factors, we describe this component as a general protein p, representing the average effector cytotoxicity and given by Eq. E, where μ_3 is natural degradation of p within the biological ranges, and b_1 and b_2 are variables of the chosen function. The initial condition is $p_0 = p(t = 0)$.

Tumor dynamics. To allow for *in vivo* tumor growth as affected by natural immune responses that differ for immunogenically varying cancers (1), the function $g(n)$ (Eq. F), standing for the dynamics of tumor cell number, n, in normal untreated mice, is constructed separately for each tumor type according to the observed growth curves (see Parameter Estimation). Tumor progression is assumed to be affected by the cytotoxic, p-mediated, antitumor activity of $CD8^+$ T and NK cells, affinities of tumor and NK or $CD8^+$ T-cell interactions being represented by k_1 and k_2, respectively.

As experiments evaluate tumor size by measuring tumor surface, Eq. F is modified to allow a simple transformation between these quantities. Based on observations that tumor cells, inoculated in a solution, develop a defined shape within a few days (5, 6),[1] the corresponding simplified evaluation of initial tumor surface is to divide the number of injected cells by the scale of a tumor cell surface, 10^{-6} mm^2, so that, for instance, 10^5 cells will correspond to a size of 0.1 mm^2. Secondly, the tumor is thought to evolve as a homogenous sphere with a constant density volume, allowing tumor volume, and tumor cell number (n), to be proportional to $z^{3/2}$. Using the scale law, $n \sim z^{3/2}$, and skipping the irrelevant coefficient, Eq. F is transformed into

$$\dot{z} = z^{-1/2} g(z^{3/2}) - k_1 pxz - k_2 pyz. \quad \text{(J)}$$

Considering standard experimental methods, the initial condition is defined as $z_0 = z(t = 0)$.

Collectively, the above equations constitute an autonomous ODE system. The positivity of the solutions, corresponding to positive initial conditions, is easily verified. Moreover, the immune system components x and y are always confined to the biological relevant strip $[x_{\min}, x_0] \times [y_0, y_\infty]$.

Parameter Estimation

IL-21 dynamics. As tumor size is estimated through surface measurements, rather than through cell number, IL-21 dynamics (Eq. I) are modified to

$$\dot{u} = hz^{3/2} - \mu_1 u. \quad \text{(K)}$$

Because 10^5 genetically modified tumor cells were found to produce ~2 ng/mL IL-21 in 1 day (5), the constant h may be retrieved. Simply, if tumor size is assumed unchanged within the first day, and IL-21 concentration at the initial time is 0, IL-21 is estimated by

$$\dot{u} \sim hz_0^{3/2} - \mu_1 u. \quad \text{(L)}$$

Eq. K, together with the conditions $u(0) = 0$ and $u(\tilde{t} = 1\ \text{day}) = 2$ ng/mL gives

$$u(\tilde{t}) = \frac{hz_0^{3/2}}{\mu_1}[1 - exp(-\mu_1 \tilde{t})], \quad \text{(M)}$$

so that

$$h = \frac{\mu_1 u(\tilde{t})}{z_0^{3/2}(1 - e^{-\mu_1 \tilde{t}})}. \quad \text{(N)}$$

Given the values $z_0 \sim 10^{-1}$ mm^2, $\mu_1 = 10$ $days^{-1}$, $\tilde{t} \sim 1$ day, h is estimated at 6.34×10^2 $mm^{-3/2}$ ng mL^{-1} $days^{-1}$.

As discussed previously, for HGD and SID, the *input* function forms a pulse whose amplitude corresponds to the given dose. For SID, the exponential decay rate was only roughly estimated due to unavailability of IL-21 pharmacokinetic data. The homology of IL-21 to IL-2 (4), whose decay rate is a few hours (34), suggested a similar value for IL-21 (μ_1 = 10 $days^{-1}$). Conversely, IL-21 kinetics in HGD (Fig. 2*A*) were evaluated by exponentially fitting IL-21 concentrations from the experimental assay (13). Here, μ_1 was approximated at a much lower rate (0.58 $days^{-1}$) due to continuous durable production of IL-21 in this method. In HGD simulations, administration will be delayed by a day with respect to experiments, because plasma IL-21 levels were measured only 24 hours following injection.

NK-cell dynamics. Parameters for NK-cell growth under no treatment were determined first. The carrying capacity was set to $x_0 = 1.95 \times 10^6$ cells, an average of the NK population sizes in untreated mouse spleens (13). To estimate r_1, turnover rates of NK cells were required, yet little is known regarding these rates in cancerous conditions. Healthy mature mice or primates show a daily NK renewal rate of ~2% to 5% (26, 35),

[1] Dr. Margery Ma (Wyeth Pharmaceuticals), personal communication.

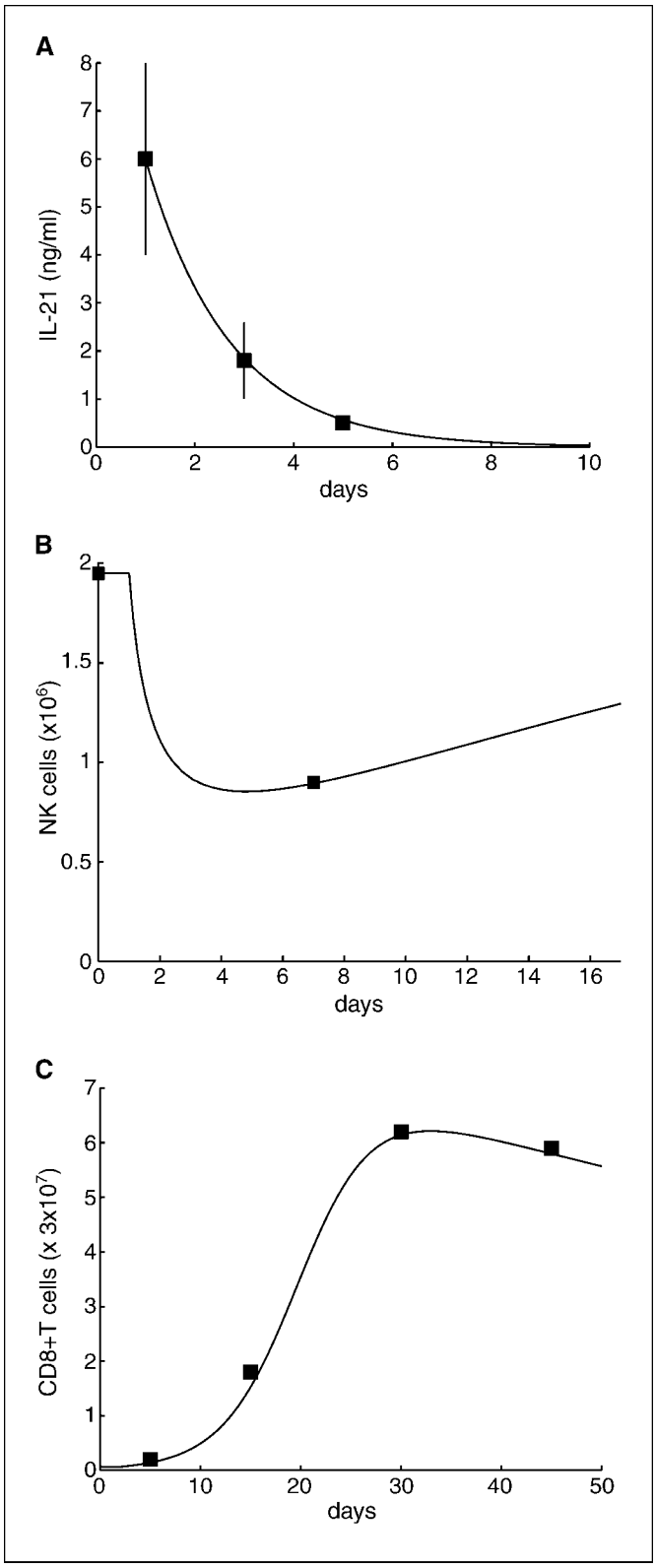

Figure 2. Fits of IL-21, NK-cell, and CD8$^+$ T-cell dynamics to experimental results. *A,* IL-21 dynamics following injection of 20 μg HGD plasmids were reproduced according to experimental measurements (*filled squares*; 13). *B,* NK-cell dynamics in context of the above drug administration were retrieved by interpolating two experimental points at days 0 and 7 (*filled squares*) from the same study. *C,* CD8$^+$ T-cell dynamics retrieving the experimental points at days 5, 15, 30, and 45 (*filled squares*) in a different experiment (7), where SID of IL-21 was applied (six 10 μg/mL injections at days 2, 4, 6, 8, 10, and 12).

which increases in presence of antigen. Hence, r_1 is set so that the NK-cell replacement rate does not exceed 10% per day. Following strong reduction in NK-cell numbers, their dynamics can be approximated by an exponential growth, and the ratio between population sizes of 2 consecutive days is e^{r_1}. A daily increment of 10% ($e^{r_1} = 1.1$) allows to calculate $r_1 = \log(1.1)$. Near the carrying capacity, where the approximation of an exponential law is no longer valid and growth is slower, this percentage is generally decreased. For parameter, p_1, denoting the lower threshold for NK numbers, a value within a biological range (10^4 cells) is designated.

IL-21-mediated NK-cell decrease was evaluated based on an *in vivo* murine HGD study where splenic NK cells were counted 1 week after IL-21 administration in a noncancerous setting (13). IL-21 dynamics in HGD were applied to evaluate the parameters under which the function $h_1(u)$ interpolates the two experimental points (Fig. 2*B*). The resulting values for p_2 and q_1 were 1.054×10^6 and 0.54×10^6 cells, respectively.

CD8$^+$ T-cell dynamics. To determine parameters of IL-21-affected dynamics of CD8$^+$ T cells, we used a study evaluating the response to i.p. injections of murine IL-21 in a thymoma line (7). Here, six 20 μg doses (equivalent to 10 μg/mL for a 2 mL murine blood volume) were given on alternate days, decay rate being $\mu_1 = 10$ days^{-1}, and CD8$^+$ T cells were counted in draining lymph nodes (DLN) on days 5, 15, 30, and 45. To evaluate the initial number of specific CD8$^+$ T cells, we assumed an initial exponential growth as suggested by the global behavior. The resulting curve enabled to determine the exponential factor r_2 (at a value of 0.26 days^{-1}) and consequently lead to a rough approximation of the initial condition as 0.06% of DLN CD8$^+$ T cells.

A maximum percentage of specific CD8$^+$ T-cell clones in the lymph nodes was set to 10% of DLN cells ($y_\infty = \sigma D = 3 \times 10^6$ cells = 10% of 3×10^7 cells). The maximum was configured at ~5% to 6% of 3×10^7 cells at day 30,[2] allowing separate evaluation of D and σ. These latter two variables depend on the specific tumor type, as this ability is expected to be more pronounced in more immunogenic types. Due to scarcity of experiments for analyzing the CD8$^+$ T-cell dynamics for a nonimmunogenic model, values are roughly set in the ranges $\sigma = [0.002, 0.008]$ cells ng mL^{-1} and $D = [0.19 \times 10^3, 1.4 \times 10^3]$ ng mL^{-1}. Finally, μ_2, the clearance parameter of m, is set to 0.014 days^{-1}, as the duration of the response was ~100 days (5, 7), and a is set as 0.57, to fit experimental data (Fig. 2*C*).

Cytotoxic protein dynamics. Lytic activity is elevated up to several weeks after primary challenge of genetically modified tumor cells in CGT (5, 6) and normal tumor cells in HGD or SID (7, 13). Therefore, parameters were fixed so that μ_3^{-1} is in the range of tens of days. The concentration at saturation, b_2, is set to 0.1 ng mL^{-1}. This constant, along with b_1 (set as 10^{-1} days ng mL^{-1}), is evaluated by curve fitting.

Tumor dynamics. To describe the nonimmunogenic B16 melanoma growth function in control mice (5, 13), a logistic growth was assumed for the total number of tumor cells. Using the scaling law, $n \sim z^{3/2}$, this corresponds to the tumor surface

$$\dot{z} = r_3 z\left(1 - \frac{z^{3/2}}{K}\right), \qquad \text{(O)}$$

which was fit with the observed data (Fig. 3*A*). For immunogenic MethA fibrosarcoma (5), a linear growth for the tumor surface

$$\dot{z} = c, \qquad \text{(P)}$$

enabled an accurate fit of the growth in control mice (Fig. 3*B*). It seems, then, that for such a model, tumor cell growth function should obey a power law (36) whose exponent is 1/3. Moderately immunogenic MCA205 fibrosarcoma (13) was adequately described by an exponential growth (Fig. 3*C*). For all tumor lines, affinity variables k_1 and k_2 were evaluated to retrieve experimental dynamics.

[2] Dr. Protul A. Shrikant (Roswell Park Cancer Institute), personal communication.

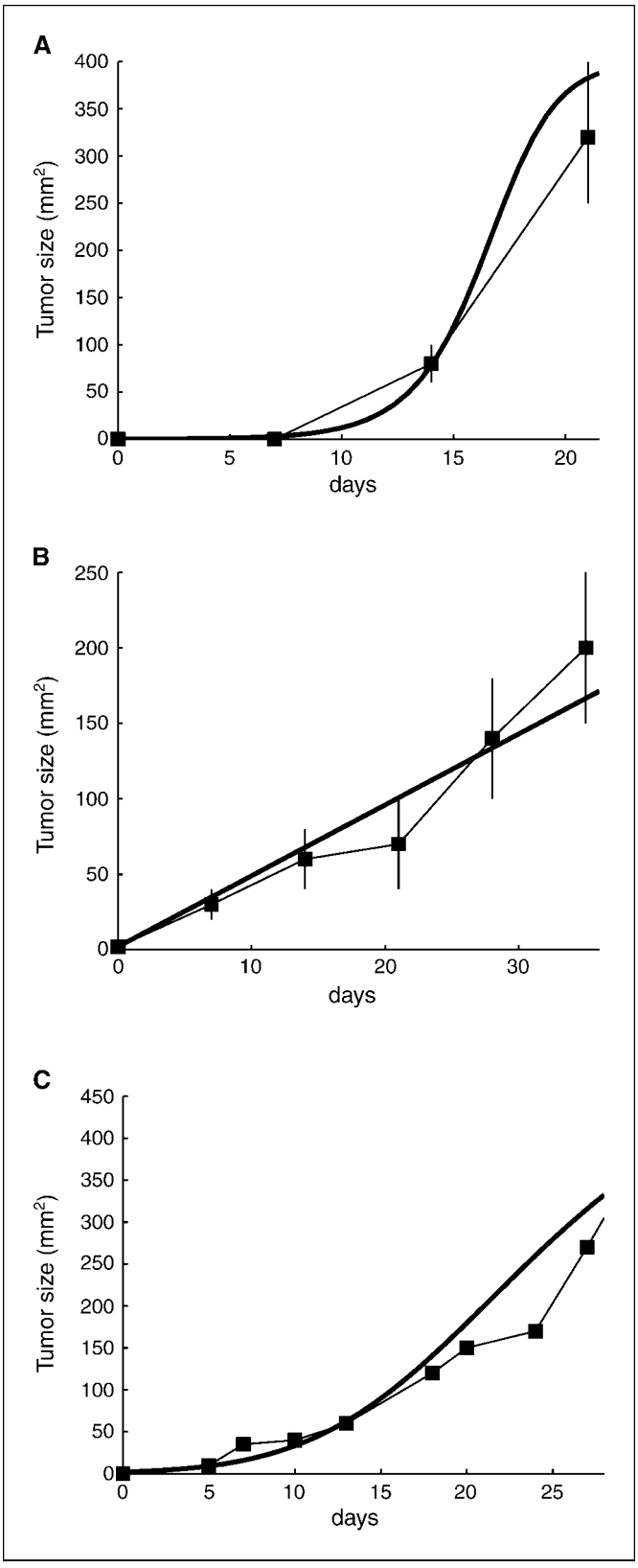

Figure 3. Fits of experimental tumor growth in control mice. B16 melanoma (*A*) was selected as a modified logistic growth retrieving a previous experiment (5). Similarly, MethA fibrosarcoma (*B*) was described by a linear growth (5), and MCA205 fibrosarcoma (*C*) was selected as an exponential growth (13). Dynamics of the interpolating curves (*thick lines*) are shown in comparison with experimental dynamics (*thin lines*).

Results

First, the model was evaluated by its robustness in retrieving experimental growth curves of tumors that differ in immunogenic pattern and under different IL-21 administration routes. Results show that parameters successfully recovering immunogenic fibrosarcoma are similar to those that recover nonimmunogenic melanoma, varying mildly in tumor-specific immunity only (see Supplementary Data). Subsequently, we examined different strategies of SID therapy of IL-21 for cancers of varying immunogenicity and growth dynamics.

Model retrieval of CGT experiments. In the first experiment (5), inoculation of an immunogenic MethA IL-21-secreting fibrosarcoma (2×10^6 cells at day 0) resulted in nonmonotonic tumor growth (Fig. 4*A, filled circles*). These dynamics seemed comparable with tumor growth in untreated mice during the first week (Fig. 4*A, filled squares*) yet decreased thereafter toward complete elimination. This immunogenic scenario (5) was reproduced in the model (Fig. 4*A, thick line*), assuming (*a*) a high $CD8^+$ T-cell effect, roughly reflected by $k_2\sigma D$, the combined affinity and carrying capacity values, and (*b*) a low affinity for the NK tumor-killing interaction as suggested by the strong NK inhibition in highly immunogenic tumors (1, 37). Simulations showed an initial rapid tumor cell increase due to lack of lysis in early stages of the response. The resulting high IL-21 concentrations lead to $CD8^+$ T-cell proliferation and subsequent tumor eradication. The simulated behavior complied with experimental curves and with the observation that full immune control of the tumor was accomplished within ~ 3 weeks.

The second experiment, in which 10^5 cells of a nonimmunogenic B16 IL-21-secreting melanoma were inoculated at day 0 (5), was also investigated by the mathematical model. In this experiment, complete elimination of the tumor was achieved in treated mice (Fig. 4*B, filled circles*) compared with control mice (Fig. 4*B, filled squares*), but data were not sufficient for characterizing the exact tumor dynamics. Still, experimental tumor development was minor and limited to the first 7 days following treatment initiation.[1] Model simulations with a low $CD8^+$ T-cell effect and a high NK tumor affinity value achieved similar results of minimal or no tumor growth (Fig. 4*B, thick line*).

Experimental CGT results, showing effective cancer regression, suggest that the exact IL-21 concentrations in this method can be of therapeutic significance. A model-independent analysis of the previously reported IL-21 production rates in CGT (5) tested this possibility: In fibrosarcoma, the IL-21 intensity measured by $v = \int_0^t u(s)ds$ was calculated at ~ 30 μg mL^{-1} days for the first 20 days of therapy. This implies that mean levels of circulating IL-21 during the antitumor activity are in the order of 1 μg/mL. In contrast, evaluation of mean IL-21 levels in B16 melanoma was problematic due to imprecise tumor mass measurements. Nevertheless, a value of ~ 10 ng/mL during the first therapeutic week is reasonable in this tumor line. This discrepancy suggests different requirements for IL-21-mediated elimination of immunogenically varying tumors.

Our model was used to retrieve experiments of immunodeficient mice challenged with IL-21-secreting B16-melanoma (5). In our simulations, each effector type was "knocked out" by setting the corresponding tumor affinity to 0. Model simulations (Fig. 4*C* and *D, thick lines*) agreed with experimental curves (Fig. 4*C* and *D, filled squares*), where the IL-21-induced antitumor effect was significantly decreased in abrogation of NK or $CD8^+$ T cells. However, different dynamics were observed for each case: Tumor growth under $CD8^+$ T-cell depletion, delayed at first, was accelerated later on, whereas

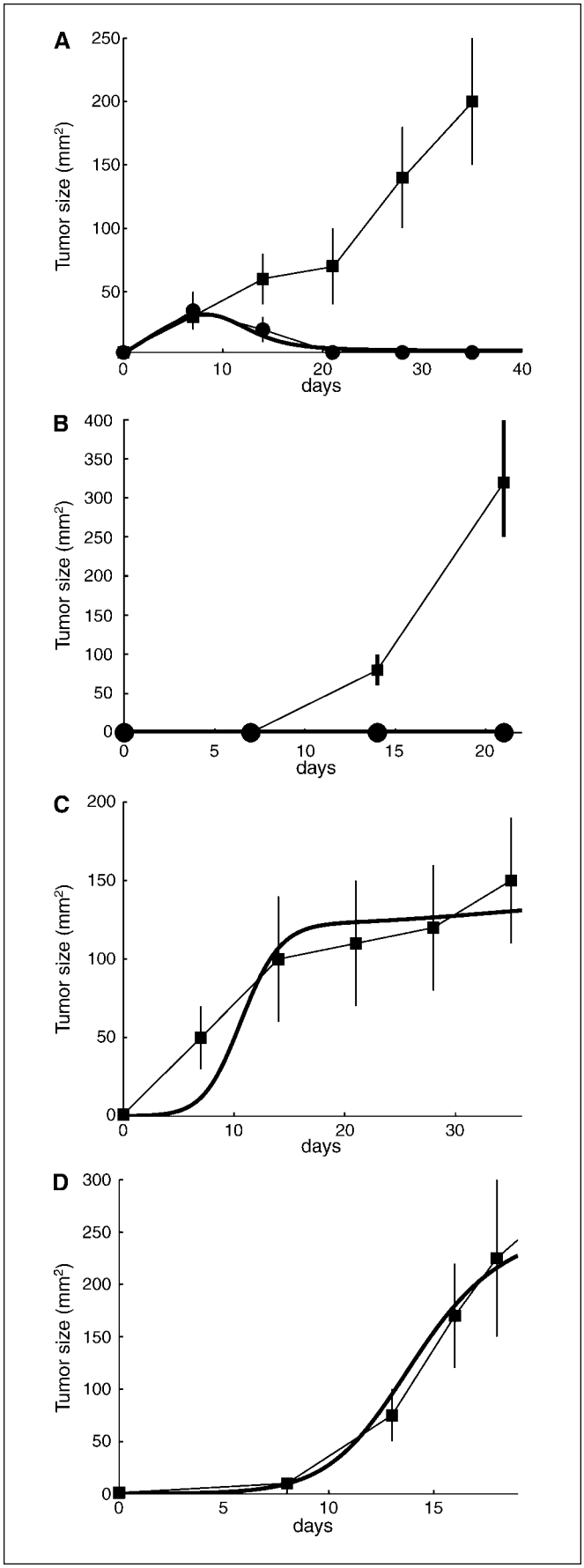

in NK-depleted mice the opposite behavior was seen. Of note, tumor-effector affinity values, derived from both depletion simulations (Fig. 4*C* and *D*), yielded tumor growth (data not shown) similar to the experimental melanoma growth curves in normal IL-21-treated mice (Fig. 4*B*). Thus, in our model, any reciprocal interactions between NK and $CD8^+$ T cells in the IL-21-treated scenario, if such exist, are likely subsumed into the independent effector dynamics, supporting the exclusion of their explicit description in the current model.

Model retrieval of HGD experiments. We retrieved elimination of a nonimmunogenic B16 melanoma and a moderately immunogenic MCA205 fibrosarcoma via i.v. gene delivery of IL-21 (13). In the experiment, two 20 μg IL-21-expressing plasmids were given in days 5 and 12 following tumor inoculation (5×10^5 cells), and IL-21 concentrations followed previously described kinetics (Fig. 2*A*). Simulation results show that the tumor-specific parameters, derived above for CGT, were sufficient for mimicking melanoma dynamics in HGD (Fig. 5*A*) and for leading to the appropriate change in NK-cell dynamics (Fig. 5*B*). Similarly, retrieval of fibrosarcoma growth (Fig. 5*C*) was satisfactory with tumor-effector affinity values from CGT simulations in the analogous tumor line. The average concentration of circulating IL-21 produced by the given plasmids during the first 3 weeks did not exceed 1 ng/mL, a lower value than in CGT. This result is corroborated by the limited tumor elimination shown in this HGD method compared with CGT (Fig. 4*A* and *B*). Overall, simulated growth fits experimental measurements in both tumor models described.

Model simulations of tumor-dependent IL-21 therapy. As the most effective tumor elimination was observed in tumor-dependent IL-21 therapy (Fig. 1*A*), such as CGT (5, 6, 20, 22), we used the model to simulate this treatment in immunogenically varying cancers. As CGT is clinically nonexecutable, a treatment strategy combining CGT and SID was simulated. The treatment comprised scheduled IL-21 dosing that was dynamically adjusted during therapy according to the tumor mass. In our simulations, IL-21 doses were set equivalent to the cytokine levels produced by the genetically modified tumor of the corresponding size. Our model simulated this procedure for the nonimmunogenic B16 melanoma and immunogenic MethA fibrosarcoma tumor lines, using their unique parameter sets, evaluated in the previous stages.

In the simulated melanoma (10^5 tumor cells inoculated), a regimen of 10 daily injections resulted in notable tumor rejection (Fig. 6*A*), dose intensities remaining in the range of nanogram per milliliter (Fig. 6*B*). The IL-21-mediated NK-cell inhibition was lower in the exogenous CGT-resembling therapy than in original CGT, coinciding with the lower total IL-21 levels used in this regimen (data not shown). Notwithstanding, the simulated tumor remained controlled for several weeks as in CGT (Fig. 4*B*). In contrast, simulating application of the same treatment regimen to immunogenic MethA fibrosarcoma (2×10^6 tumor cells inoculated) resulted in incomplete tumor elimination (Fig. 6*C*), although the given IL-21 doses reached maximum values of 10 μg/mL (Fig. 6*D*). These results

Figure 4. Simulations retrieving experimental fibrosarcoma and melanoma dynamics following IL-21 administration via CGT in normal and immunodeficient mice (5). *A,* immunogenic MethA fibrosarcoma growth following experimental IL-21-CGT therapy in normal mice (*thin line, filled circles*) is reproduced by the model simulations (*thick line*). *B,* nonimmunogenic B16 melanoma growth under similar drug application (*filled circles*) is simulated (*thick line*). Tumor growth in control mice is indicated in each case (*thin line, filled squares*). Experimental B16 melanoma growth in NK-cell-depleted (*C*) or T-cell-depleted (*D*) mice treated with IL-21 through CGT (*thin line, filled squares*) was similarly reproduced by model simulations (*thick line*).

indicate that both the immunogenic nature of the cancer and its size determine the success of tumor-dependent IL-21 therapy.

Discussion

In this work, we have introduced a mathematical model for *in vivo* antitumor activity of IL-21 in mice. Our model, focusing on NK- and T-cell immunity, was motivated by the irrefutable role of these cells in the IL-21-induced cancer control (2, 12). The robustness of the model was shown by its success in retrieving experimental growth dynamics of various tumor types, using a narrow range of parameters, and by reflecting well-established properties of cell-mediated antitumor immunity. Thus, a high correlation between tumor immunogenicity and effector balance was shown in the simulations: Nonimmunogenic melanoma tumors required high NK-cell lytic activity, as estimated in NK-tumor affinity values. Conversely, for the highly immunogenic fibrosarcomas, a strong $CD8^+$ T-cell effect, facilitated by both tumor-effector affinity and effector carrying capacity variables, was necessary (1, 37).

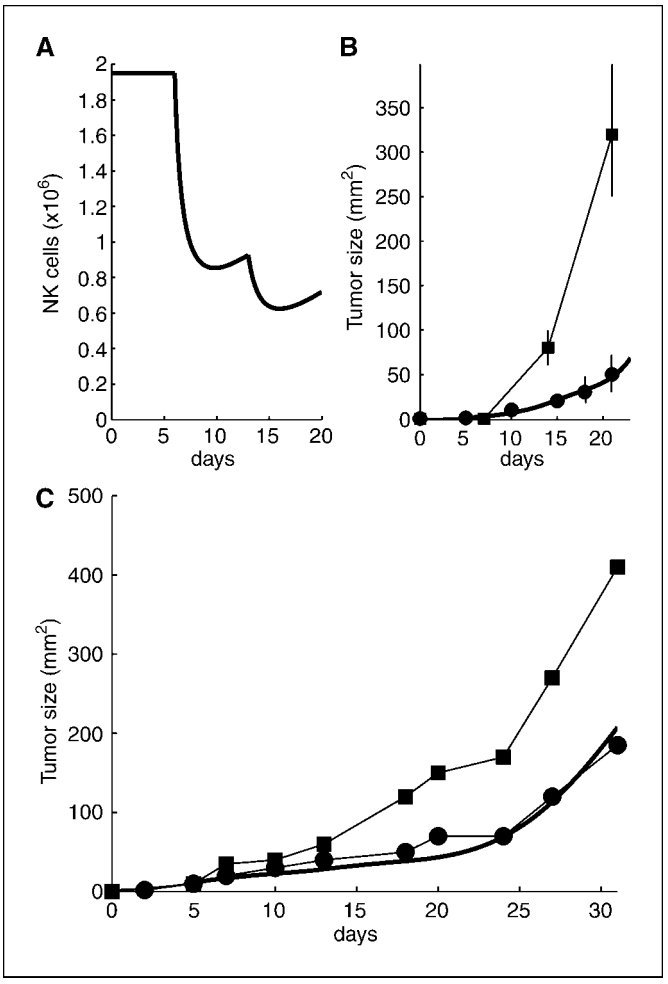

Figure 5. Simulations retrieving experimental melanoma and fibrosarcoma dynamics following IL-21 administration via HGD in mice (13). *A,* application of 20 μg IL-21-secreting plasmids at days 5 and 12 in mice inoculated with nonimmunogenic B16 melanoma resulted in tumor dynamics (*filled circles*), which served for comparison with model simulations of tumor growth under a similar regimen (*thick line*) and to experimental tumor growth in control mice (*thin line* and *filled squares*). *B,* NK-cell dynamics under this treatment. *C,* MCA205 fibrosarcoma growth in mice treated by the same regimen (*thin line* and *filled circles*) is compared with the model simulations (*thick line*) and to experimental tumor growth in control mice (*thin line* and *filled squares*).

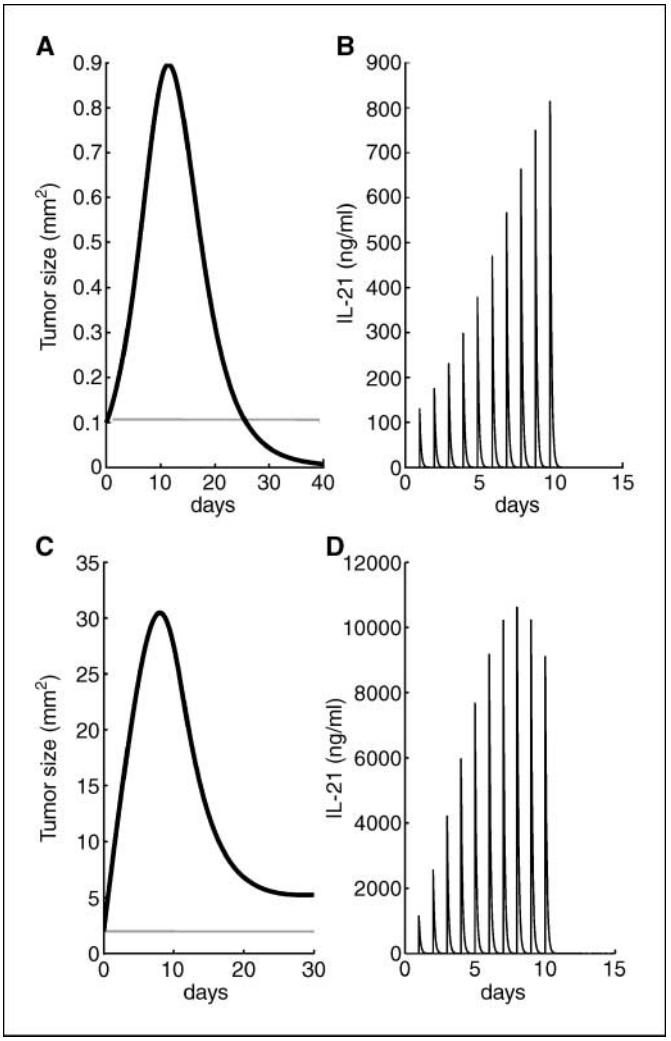

Figure 6. Simulations of CGT-like IL-21 interval dosing therapy in melanoma and fibrosarcoma. Murine B16 melanoma dynamics are predicted (*A*) in a CGT-based treatment regimen of 10 daily IL-21 i.v. injections (*B*). Murine MethA fibrosarcoma dynamics are predicted (*C*) under the same treatment regimen (*D*). *Gray horizontal lines,* threshold of initial tumor mass.

As in nonimmunogenic tumors, the activity of innate-phase effectors seems crucial; their destruction by the given IL-21 must be prevented. In such circumstances, IL-21 levels that are relatively low (in the range of ~10 ng/mL) seem most appropriate for small tumor mass, because IL-21 reduces the number of NK cells in a dose-dependent manner. Indeed, tumor elimination was achieved when simulating CGT-like therapy in nonimmunogenic melanoma, that is, dynamic dosing of IL-21 according to tumor mass at the time of administration.

IL-21 applied via CGT resulted in tumor extinction in several experiments (5, 6, 20, 22), whereas HGD did not remove tumor completely (13). Our calculations show that mean IL-21 levels in CGT (10-10,000 ng/mL) are significantly higher than IL-21 concentrations in HGD (~1 ng/mL). It can be argued, then, that dominating the success of CGT is the large IL-21 concentrations exerted in this method. However, this is not the case, because other administration strategies using similar or even higher IL-21 concentrations show ineffective tumor eradication (10, 23, 24). We believe that successful CGT is due to the given IL-21 dose depending on tumor mass at any moment. In this way, a more

natural stimulation of the immune response is achieved, avoiding abrogation of NK cells when innate immunity is indispensable.

Although T-cell responses are dominant in tumors of intensified immunogenicity, NK cells may contribute via indirect mechanisms that aid T-cell function (1). Investigation of fibrosarcoma dynamics in NK-cell-depleted mice treated with IL-21 can further elucidate this possibility. If NK cells are negligible in these circumstances, the use of high-dose (~ 10 μg/mL) IL-21 tumor-independent regimens, already from early disease stages, would seem a more reasonable treatment. Indeed, such drug concentrations were efficacious in a recent murine study of IL-21 therapy in an immunogenic renal cell carcinoma (25). Clinical implementation of such a strategy, however, should still scout for safety limitations as in any intensified treatment. In another work,[3] we use optimal control methods for fine-tuning the above-suggested tumor-dependent and tumor-independent immunotherapy regimens, to maximize antitumor efficacy, while minimizing putative IL-21 side effects.

Experimental investigation of cytotoxic protein (perforin and IFN-γ) elevation in various tumors under IL-21 administration (5, 6, 21, 33, 38) will illuminate possible adverse effects of this cytokine, including IL-21-mediated inflammation, whereas information on synergistic ILs (8, 23, 39) may aid in evaluating monotherapy and combination immunotherapy. This information can be transformed to biomathematical terms for fine-tuning our model, in addition to long-range effects of the drug, which can be incorporated by allowing for humoral, antimetastatic, and antiangiogenic properties of IL-21 (6, 8, 25).

IL-21 continuously exhibits therapeutic promise in its antitumor effects. Similarity of murine IL-21 interactions to the human system will substantiate the clinical implications of our findings. Validating the universality of our suggested model in prospective trials will pave the way for actual recommendations of IL-21 immunotherapy strategies, based on this work.

[3] A. Cappuccio et al., submitted for publication.

Acknowledgments

Received 1/23/2006; revised 4/11/2006; accepted 5/11/2006.

Grant support: Marie Curie grant MRTN-CT-2004-503661 (A. Cappuccio) and Chai Foundation (Z. Agur and M. Elishmereni).

The costs of publication of this article were defrayed in part by the payment of page charges. This article must therefore be hereby marked *advertisement* in accordance with 18 U.S.C. Section 1734 solely to indicate this fact.

We thank Drs. Margery Ma, Vladimir Vainstein, Natalie Kalev-Kronik, Yuri Kogan, and Protul A. Shrikant for valuable discussions and comments.

References

1. Janeway CA, Travers P, Walport M, Shlomchik M. Immunobiology. 6th ed. New York: Garland Science; 2005.

2. Sivakumar PV, Foster DC, Clegg CH. Interleukin-21 is a T-helper cytokine that regulates humoral immunity and cell-mediated anti-tumour responses. Immunology 2004; 112:177–82.

3. Mehta DS, Wurster AL, Grusby MJ. Biology of IL-21 and the IL-21 receptor. Immunol Rev 2004;202:84–95.

4. Parrish-Novak J, Dillon SR, Nelson A, et al. Interleukin 21 and its receptor are involved in NK cell expansion and regulation of lymphocyte function. Nature 2000;408: 57–63.

5. Ma HL, Whitters MJ, Konz RF, et al. IL-21 activates both innate and adaptive immunity to generate potent antitumor responses that require perforin but are independent of IFN-γ. J Immunol 2003;171:608–15.

6. Di Carlo E, Comes A, Orengo AM, et al. IL-21 induces tumor rejection by specific CTL and IFN-γ-dependent CXC chemokines in syngeneic mice. J Immunol 2004; 172:1540–7.

7. Moroz A, Eppolito C, Li Q, Tao J, Clegg CH, Shrikant PA. IL-21 enhances and sustains $CD8^+$ T-cell responses to achieve durable tumor immunity: comparative evaluation of IL-2, IL-15, and IL-21. J Immunol 2004; 173:900–9.

8. Kishida T, Asada H, Itokawa Y, et al. Interleukin (IL)-21 and IL-15 genetic transfer synergistically augments therapeutic antitumor immunity and promotes regression of metastatic lymphoma. Mol Ther 2003;8:552–8.

9. Nutt SL, Brady J, Hayakawa Y, Smyth MJ. Interleukin 21: a key player in lymphocyte maturation. Crit Rev Immunol 2004;24:239–50.

10. Takaki R, Hayakawa Y, Nelson A, et al. IL-21 enhances tumor rejection through a NKG2D-dependent mechanism. J Immunol 2005;175:2167–73.

11. Parrish-Novak J, Foster DC, Holly RD, Clegg CH. Interleukin-21 and the IL-21 receptor: novel effectors of NK and T cell responses. J Leukoc Biol 2002;72:856–63.

12. Habib T, Nelson A, Kaushansky K. IL-21: a novel IL-2-family lymphokine that modulates B, T, and natural killer cell responses. J Allergy Clin Immunol 2003;112: 1033–45.

13. Wang G, Tschoi M, Spolski R, et al. *In vivo* antitumor activity of interleukin 21 mediated by natural killer cells. Cancer Res 2003;63:9016–22.

14. Nakano H, Kishida T, Asada H, et al. Interleukin-21 triggers both cellular and humoral immune responses leading to therapeutic antitumor effects against head and neck squamous cell carcinoma. J Gene Med 2006;8: 90–9.

15. Agur Z, Arnon R, Schechter B. Reduction of cytotoxicity to normal tissues by new regimens of phase-specific drugs. Math Biosci 1988;92:1–15.

16. Arakelyan L, Merbl Y, Agur Z. Vessel maturation effects on tumour growth: validation of a computer model in implanted human ovarian carcinoma spheroids. Eur J Cancer 2005;41:159–67.

17. Skomorovski K, Harpak H, Ianovski A, at al. New TPO treatment schedules of increased safety and efficacy: pre-clinical validation of a thrombopoiesis simulation model. Br J Haematol 2003;123:683–91.

18. De Pillis LG, Radunskaya AE, Wiseman CL. A validated mathematical model of cell-mediated immune response to tumor growth. Cancer Res 2005; 65:7950–8.

19. De Pillis LG, Gu W, Radunskaya AE. Mixed immunotherapy and chemotherapy of tumors: modeling, applications and biological interpretations. J Theor Biol. Epub 2005 Sep 6.

20. Ugai S, Shimozato O, Kawamura K, et al. Expression of the interleukin-21 gene in murine colon carcinoma cells generates systemic immunity in the inoculated hosts. Cancer Gene Ther 2003;10:187–92.

21. Brady J, Hayakawa Y, Smyth MJ, Nutt SL. IL-21 induces the functional maturation of murine NK cells. J Immunol 2004;172:2048–58.

22. Ugai S, Shimozato O, Yu L, et al. Transduction of the IL-21 and IL-23 genes in human pancreatic carcinoma cells produces natural killer cell-dependent and independent antitumor effects. Cancer Gene Ther 2003;10: 771–8.

23. Zeng R, Spolski R, Finkelstein SE, et al. Synergy of IL-21 and IL-15 in regulating $CD8^+$ T cell expansion and function. J Exp Med 2005;201:139–48.

24. Nelson A, Hughes S, Sivakumar P, et al. Interleukin 21 enhances tumor specific immunity [abstract]. Proc Am Soc Clin Oncol 2003;22:171.

25. Hughes S, Chin L, Waggie K, Sivakumar P, Everson C, Clegg C. Interleukin 21 efficacy in a mouse model of metastatic renal cell carcinoma [abstract]. J Clin Oncol (Meet Abstr) 2004;22:2598.

26. Jamieson AM, Isnard P, Dorfman JR, Coles MC, Raulet DH. Turnover and proliferation of NK cells in steady state and lymphopenic conditions. J Immunol 2004;172:864–70.

27. Toomey JA, Gays F, Foster D, Brooks CG. Cytokine requirements for the growth and development of mouse NK cells *in vitro*. J Leukoc Biol 2003;74:233–42.

28. Kasaian MT, Whitters MJ, Carter LL, et al. IL-21 limits NK cell responses and promotes antigen-specific T cell activation: a mediator of the transition from innate to adaptive immunity. Immunity 2002;16:559–69.

29. van Leeuwen EM, Gamadia LE, Baars PA, Remmerswaal EB, ten Berge IJ, van Lier RA. Proliferation requirements of cytomegalovirus-specific, effector-type human $CD8^+$ T cells. J Immunol 2002;169:5838–43.

30. Li Y, Bleakley M, Yee C. IL-21 influences the frequency, phenotype, and affinity of the antigen-specific CD8 T cell response. J Immunol 2005;175: 2261–9.

31. Eberl M, Engel R, Beck E, Jomaa H. Differentiation of human γ-δ T cells towards distinct memory phenotypes. Cell Immunol 2002;218:1–6.

32. Seo N, Tokura Y. Downregulation of innate and acquired antitumor immunity by bystander γδ and αβ T lymphocytes with Th2 or Tr1 cytokine profiles. J Interferon Cytokine Res 1999;19:555–61.

33. Strengell M, Sareneva T, Foster D, Julkunen I, Matikainen S. IL-21 up-regulates the expression of genes associated with innate immunity and Th1 response. J Immunol 2002;169:3600–5.

34. Kirschner D, Panetta JC. Modeling immunotherapy of the tumor-immune interaction. J Math Biol 1998;37: 235–52.

35. De Boer RJ, Mohri H, Ho DD, Perelson AS. Turnover rates of B cells, T cells, and NK cells in simian immunodeficiency virus-infected and uninfected rhesus macaques. J Immunol 2003;170:2479–87.

36. Hart D, Shochat E, Agur Z. The growth law of primary breast cancer as inferred from mammography screening trials data. Br J Cancer 1998;78:382–7.

37. Glas R, Franksson L, Une C, et al. Recruitment and activation of natural killer (NK) cells *in vivo* determined by the target cell phenotype. An adaptive component of NK cell-mediated responses. J Exp Med 2000;191:129–38.

38. Pelletier M, Bouchard A, Girard D. *In vivo* and *in vitro* roles of IL-21 in inflammation. J Immunol 2004;173: 7521–30.

39. Strengell M, Matikainen S, Siren J, et al. IL-21 in synergy with IL-15 or IL-18 enhances IFN-γ production in human NK and T cells. J Immunol 2003;170:5464–9.